JOURNAL GEOLOGICAL SOCIETY OF INDIA
Vol.94, July 2019, pp.53-61

# Palaeo-weathering Characteristics and Nature of Source Lithology of a Carbonaceous Metasedimentary Unit in the Dalma Volcano-sedimentary Belt, North Singhbhum Mobile Belt, Eastern India

Mousoma Khatun, Sahendra Singh* and Rajarshi Chakravarti

Department of Applied Geology, Indian Institute of Technology (Indian School of Mines), Dhanbad - 826 004, India
***E-mail:*** *mousomakhatun@gmail.com; sahendra@iitism.ac.in*; raj41090@gmail.com*

## ABSTRACT

**The Palaeo to Mesoproterozoic Dalma volcano-sedimentary basin (DVSB) is a typical greenstone belt sequence within the North Singhbhum Mobile Belt (NSMB) of Singhbhum Crustal Province (SCP), eastern India. The volcano-sedimentary belt is situated in the central portion of NSMB and separates the Chaibasa and Dhalbhum formation lying at its south from the Chandil Formation at its north. The metasedimentary unit comprises carbonaceous phyllite, carbonaceous cherty quartzite, quartz mica schist and quartzite. In the present work, the Au-rich carbonaceous metasedimentary rocks were studied to understand the source rocks characteristic, paleoweathering history and possible tectonic set-up. Geochemical classification diagrams based on the major oxide data indicates that these units belong to arkose to wacke field and the protolith underwent moderate to high degree of chemical weathering. Based on critical elemental ratios, it is inferred that the sediments were subjected to moderate degree of physical weathering, associated with sediment sorting and recycling. A fractionated REE pattern coupled with prominent negative Eu anomaly and elevated Th/Sc ratios indicate a felsic provenance for these metasedimentary units. The data further suggests that the sediments were deposited in a passive margin tectonic setting, during a prolonged period of upliftment and erosion of the Archean Singhbhum granite complex.**

## INTRODUCTION

The NSMB is a 200 km east-west trending arcuate belt lying between the Archean cratonic core region (ACCR) in the south and Meso to Neo-Proterozoic (1.7Ga-0.9 Ga) Chhotanagpur granite gneissic complex (CGGC) at its north in the eastern Indian Shield (EIS). The entire mobile belt from south to north has been broadly subdivided into five litho tectonic domains, viz. Dhanjori Formation, Dhalbhum Formation, Chaibasa Formation, Dalma Formation (study area) and the Chandil Formation (Mahadevan 2002); and all of them have been explored previously for their gold potential (Jha et al. 2015; Chakravarti et al. 2018; Khatun and Singh. 2018). The study area belongs to the northern fringe of the DVSB (domain IV) within the NSMB, and represents a typical greenstone belt sequence (Gupta et al., 1982, 2000). The metasedimentary units comprise carbonaceous phyllite, carbonaceous cherty quartzite, quartz mica schist and quartzite with their metamorphic grade varying from greenschist to amphibolite facies (Dunn and Dey 1942). Based on the structural patterns and geochemical signatures, a mantle plume activated intercontinental rift setting has been proposed by previous workers, for the evolution of this belt (Gupta et al. 1982; Mukhopadhaya 1990,1994; Errikson et al. 1999; Mazumder 2000; Roy et al. 2002b; Mazumdar 2003). Mantle upwelling over this greenstone belt has probably made it one of the most important metallogenetic provinces of eastern India (Zhang et al. 2008; Wan et al. 2010; Maurya et al. 2015). Zircon dating of the felsic volcanic rocks, lying towards the north of the DVSB yielded an age of 1.6 Ga by SHRIMP Pb-Pb method (Nelson et al. 2007).

Though the geological and geochemical investigations of these metasedimentary units were carried out by the previous workers (Dunn and Dey 1942; Gupta et al. 1982; Jha et al. 2015 Khatun and Singh 2018; Singh et al. 2018) these formations were not investigated for their source rock characteristics i.e. provenance and tectonic setting. In the present work, these metasedimentary units have been studied to ascertain the paleo-weathering characteristics, nature of source rocks, and its implication on the tectonic evolution of the area. The effects of post-depositional alterations have been taken into consideration for geochemical interpretations.

## GEOLOGY OF THE STUDY AREA

The DVSB is an arcuate ridge situated in the middle of the NSMB (Fig.1a). The DVSB has a synclinal structure with a total strike length of 200 km and a width varying from 3 to 7 km (Mahadevan 2002). This volcano-sedimentary belt comprises shale/phyllite, carbonaceous phyllite/tuff with interlayered basic volcanic rocks and is overlain by a thick pile of high-Mg volcaniclastic rocks and co-magmatic flows of komatiitic composition (Fig.1b). This is superposed by pillowed low-K, high-Mg tholeiites of ocean floor affinity. The DVSB is further sub-divided into upper Dalma Formation and lower Dalma Formation (Gupta et al.1982, 2000). The lower Dalma Formation overlies the Chaibasa Formation and consists of carbonaceous phyllite, tuff and quartzite interlayered with volcanic rocks, whereas the upper Dalma Formation is represented by extensive development of high magnesium volcaniclastics and komatiites (Mahadevan 2002).

## PETROGRAPHY

Detailed petrographic characterization of the carbonaceous metasedimentary units were carried out in the Ore Geology Laboratory in IIT-ISM Dhanbad. The study reveals presence of quartz, muscovite, carbonates, (mainly calcite), chlorite, epidote, zircon and dusty carbonaceous matter (Fig.2 a, b, c,). The carbonaceous matter appears as wisps, diffused and at some places it appears as crystalline though partially flattened wisps in carbonaceous matter are common. Quartz veins within these rocks exhibit variable thickness varying from few mm to cm and exhibits crosscutting relationship at places. Microstructural features such as ptygmatic folding, faulting and

0016-7622/2019-94-1-53/$ 1.00 © GEOL. SOC. INDIA | DOI: 10.1007/s12594-019-1266-x

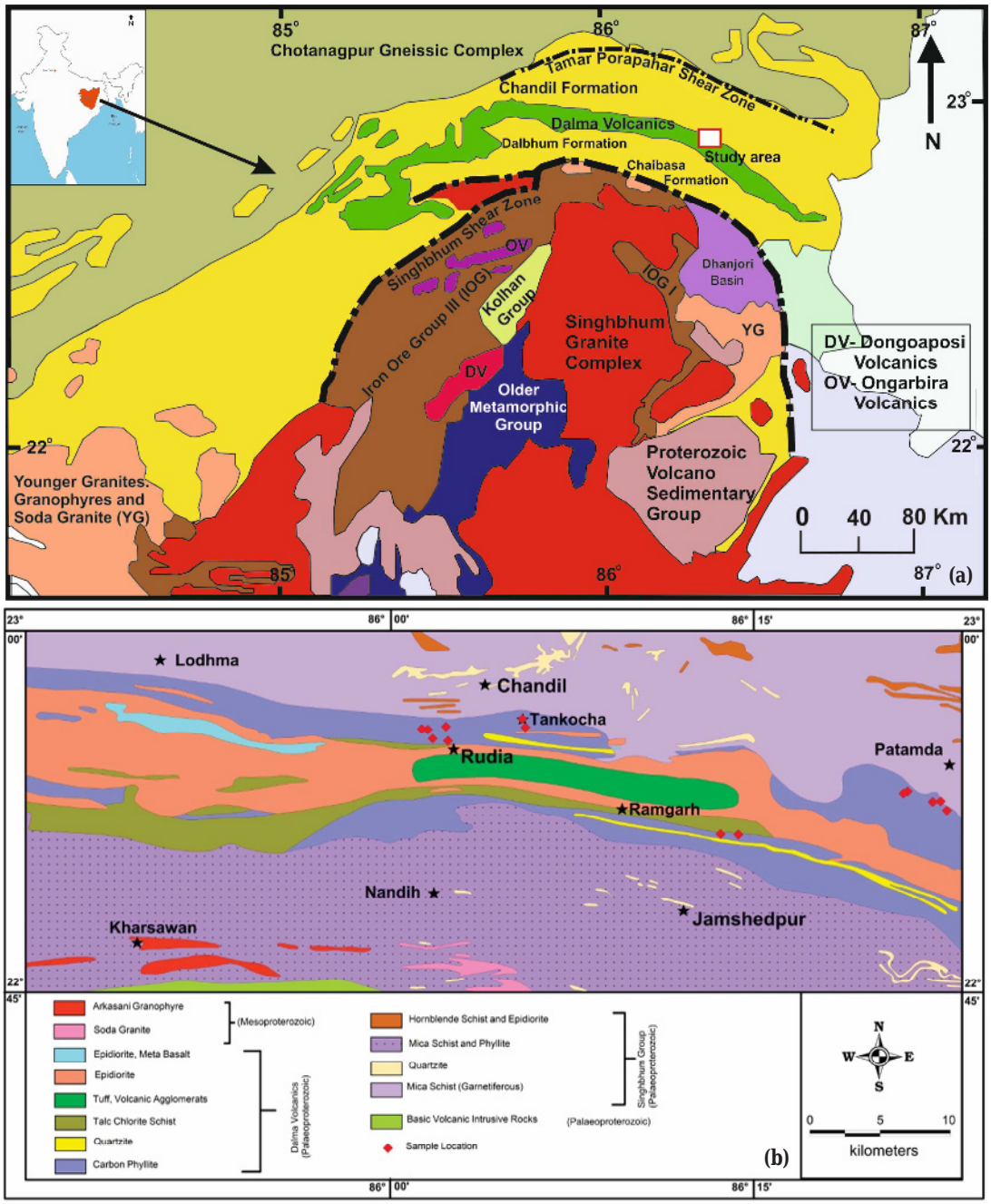


**Fig.1. (a)** Regional geological map of Singhbhum crustal province with five lithotectonic domain designated as (I, II, III, IV, V) and study area (after Geological map of India,7th edition,1998). **(b)**Geological map of study area with sample locations (after Geological quadrangle map by Geological Survey of India, 1994).

shearing of quartz vein imply that the area has undergone extensive deformation and metamorphism (Fig.2d). Ore microscopic studies of these samples indicate presence of sulphides such as pyrite, pyrrhotite, chalcopyrite, arsenopyrite and oxides like magnetite, hematite (Fig.2e).

## WHOLE ROCK GEOCHEMISTRY

Major and trace element analysis carried out using XRF and ICPMS at Bureau Veritas Commodities Ltd. Vancouver, Canada and at the sophisticated analytical instrumental facility (SAIF), IIT Bombay.

### Analytical Methodology

Major and trace element analysis were performed by the LF 200 methodology. For sample preparation rock samples were jaw crushed and were pulverized in an agate bowl for getting 400 mesh fine powder.Each powdered sample was fused using lithium borate and the melt produced was completely dissolved in hot Aqua Regia. Major and trace (Ba, Ni, Sc, Yand Zr) elements were analyzed in the resulting solution by inductively coupled plasma-optical emission spectrometry (ICP-OES detection limit: major elements~0.01%; trace elements=0.1-5.0 ppm). The remaining trace elements,including Rare Earth Elements(REE) were determined by inductively coupled plasma-mass spectrometry(ICP-MS detection limit=0.05-0.5 ppm) (Cruz-G'amez et al. 2017).

ICP-MS analysis of three samples was carried out in SAIF IITB by hydrofluoric acid method. In this method 0.2 gm of the sample is taken in a teflon beaker and 10 ml nitric acid or perchloric acid and 1 ml Hydrofluoric acid are added to it. The solution is heated on a hot plate to dryness. 10 ml of aqua-regia is then added to the dry mass and

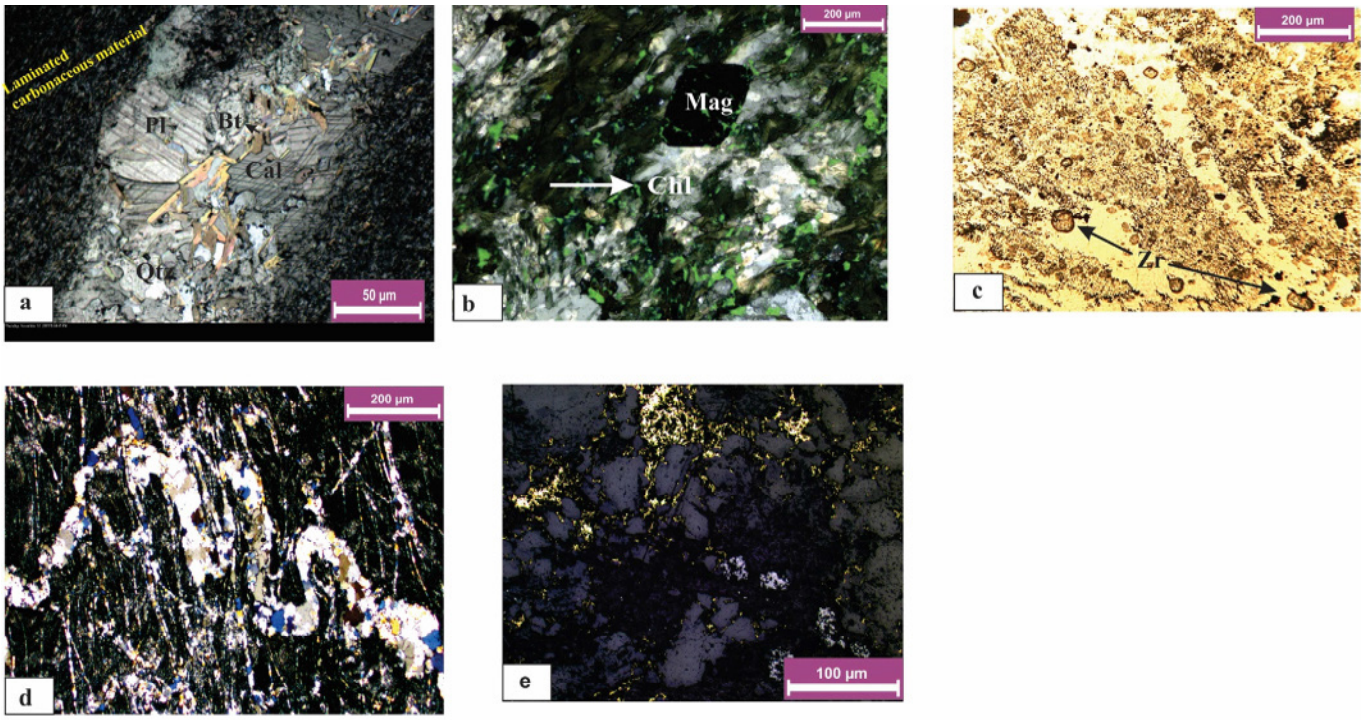


**Fig.2.** Photomicrograph showing (a) Mineral assemblage in Carbonaceous host rock (b) Occurrences of chlorite in host rock (c) Presence of zircon in host rock (d) Ptygmatic folding of quartz vein in carbonaceous host rock (e) Ore mineral presence in host rock. *Abbreviations:* Plg=Plagioclase feldspar, Cal-=Calcite, Bt=Biotite, Chl= Chlorite, Zr=Zircon, Mag=Magnetite, Cp= Chalcopyrite.

heated till everything dissolves. The solution is diluted to standard volume, 100 ml, with distilled water.

**Major Elements**

Major oxide concentrations are listed in Table 1. Harker variation diagram has been used to evaluate variation in major element geochemistry of these metasedimentary rocks. In all the 10 samples, $SiO_2$ shows positive correlation with other oxides (Fig.3a). The poor correlation of $SiO_2$ with CaO and $Na_2O$ implies mobility during weathering and metamorphism (Lima et al.,2014). Apart from the Harker variation diagrams, certain major oxides such as $K_2O$, $Na_2O$, $Fe_2O_3$ and MgO exhibit positive correlation with $Al_2O_3$ (Fig.3b) which suggests that these phases are associated with mica or clay minerals (Das et al., 2006). The major element variation was also compared with the Post Archean Australian Shale (PAAS) values (Taylor and McLennan 1985). The studied phyllites exhibit enrichment of $SiO_2$, $Al_2O_3$, MgO, $K_2O$, MnO and $TiO_2$, and depletion of $Fe_2O_3$, CaO, $Na_2O$, $TiO_2$, $P_2O_5$ compared to the PAAS composite (Fig.3c). As per the petrological and geochemical classification proposed by Herron 1988, most of the carbonaceous phyllites fall within the arkose to wacke field (Fig.3d).

***Paleo-weathering Characteristics***

In the studied samples, the Chemical Index of Alteration (CIA), ranges from 63 to 80 and are similar to typical shale weathering values (75) (Nesbitt and Young, 1982). The Chemical Index of Weathering (CIW) was also calculated for these samples, which ranges between 74 – 99 (Cullers, 2000). The CIW index is defined as the $Al_2O_3$/

**Table.1** Major element data and critical major element ratios from the sampled metasedimentary rock units (Analysis carried out at Bureau Veritas Commodities Ltd. Vancouver, Canada labotaries) and SAIF, IIT-Bombay

| Sample Number | CP-1 | CP-2 | CP-3 | CP-4 | CP-5 | CP-6 | CP-7 | CP-8 | CP-9 | CP-10 |
|---|---|---|---|---|---|---|---|---|---|---|
| $SiO_2$ (wt%) | 63.4 | 69.71 | 72.42 | 80.31 | 74.3 | 67.2 | 68.35 | 69.32 | 74.55 | 89.23 |
| $Al_2O_3$ (wt%) | 15.37 | 14.73 | 12.45 | 8.35 | 12.27 | 11.22 | 13.14 | 14.35 | 14.82 | 6.71 |
| $Fe_2O_3$ (wt%) | 1.72 | 1.27 | 0.59 | 1.25 | 1.13 | 4.68 | 2.06 | 0.55 | 0.66 | 0.2 |
| MnO (wt%) | <0.01 | <0.01 | <0.01 | <0.01 | <0.01 | 0.03 | <0.01 | 1.19 | 1.43 | 0.44 |
| MgO (wt%) | 0.96 | 0.71 | 1.15 | 0.74 | 1.19 | 4.29 | 1.54 | 8.87 | 2.38 | 0.46 |
| CaO (wt%) | 0.03 | 0.02 | 0.02 | 0.02 | 0.03 | 2.68 | 0.03 | 0.09 | 0.03 | 0.01 |
| $Na_2O$ (wt%) | 0.16 | 0.18 | 0.09 | 0.06 | 0.08 | 1.2 | 0.08 | 1.19 | 1.43 | 0.03 |
| $K_2O$ (wt%) | 4.66 | 4.12 | 4.25 | 2.88 | 4.1 | 2.59 | 4.68 | 4.12 | 4.68 | 1.58 |
| $P_2O_5$ (wt%) | 0.03 | 0.02 | 0.03 | 0.03 | 0.02 | 0.16 | 0.02 | 0.07 | 0.02 | 0.02 |
| $Cr_2O_3$ (wt%) | 0.012 | 0.013 | 0.025 | 0.02 | 0.012 | 0.01 | 0.023 | 0 | 0 | 0 |
| $TiO_2$ (wt%) | 0.68 | 0.58 | 0.62 | 0.46 | 0.74 | 0.73 | 0.63 | 0.01 | 0.02 | 0.02 |
| LOI | 12.8 | 8.4 | 8.1 | 5.5 | 5.9 | 5 | 9.2 | 0.24 | 0 | 1.3 |
| CIA | 76.01 | 77.32 | 74.06 | 73.82 | 74.45 | 63.42 | 73.28 | 72.65 | 70.70 | 80.55 |
| WIP | 39.30 | 34.80 | 35.82 | 24.23 | 34.62 | 36.17 | 39.65 | 49.74 | 48.29 | 13.33 |
| CIW | 98.77 | 98.66 | 99.12 | 99.05 | 99.11 | 74.30 | 99.16 | 91.81 | 91.03 | 99.40 |
| Si/Al | 3.64 | 4.17 | 5.13 | 8.49 | 5.34 | 5.28 | 4.59 | 4.26 | 4.44 | 11.74 |
| K/Al | 0.47 | 0.43 | 0.53 | 0.54 | 0.52 | 0.36 | 0.55 | 0.45 | 0.49 | 0.36 |
| Na/Al | 0.014 | 0.017 | 0.010 | 0.010 | 0.009 | 0.149 | 0.008 | 0.116 | 0.135 | 0.006 |

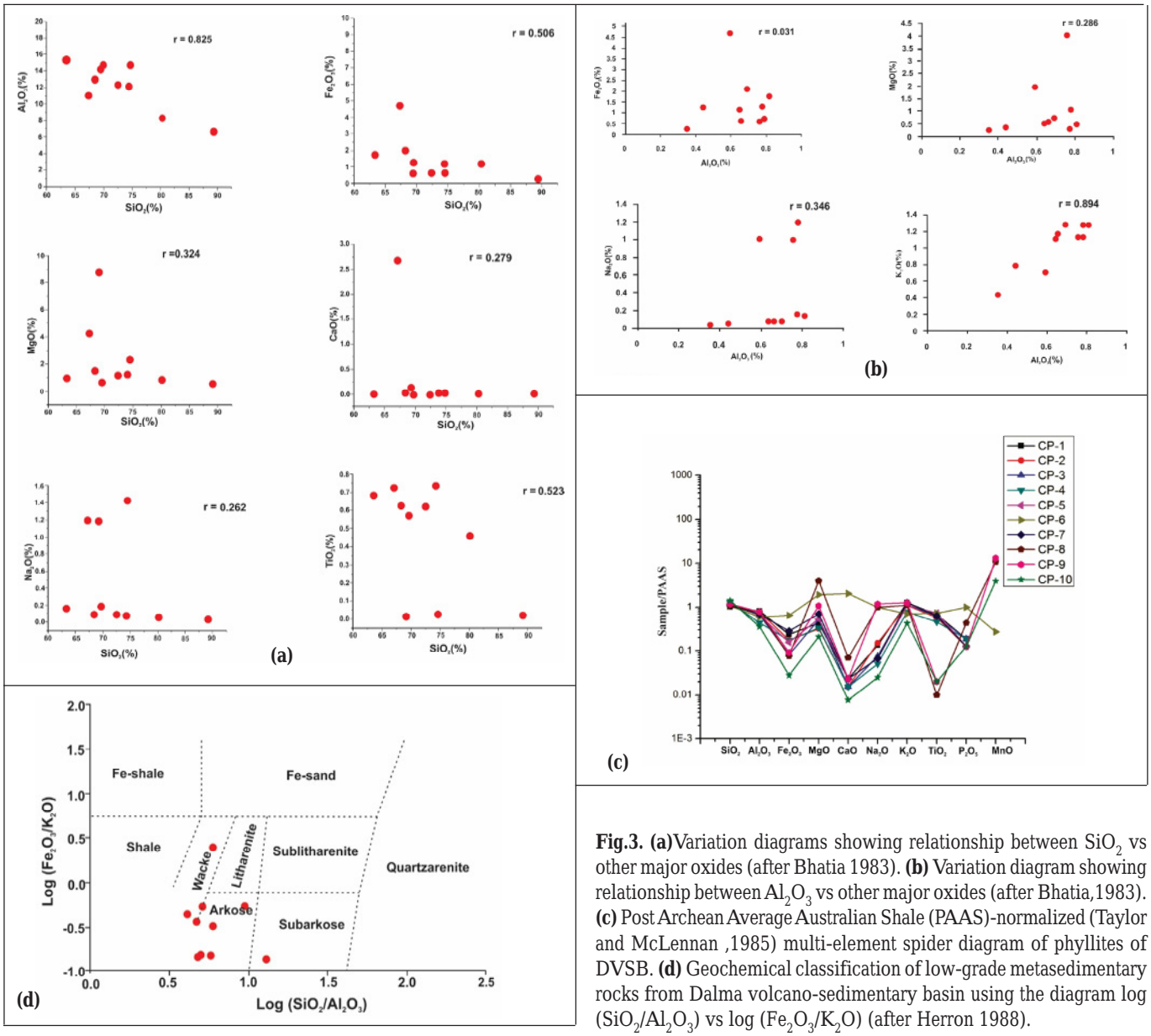


**Fig.3. (a)**Variation diagrams showing relationship between $SiO_2$ vs other major oxides (after Bhatia 1983). **(b)** Variation diagram showing relationship between $Al_2O_3$ vs other major oxides (after Bhatia,1983). **(c)** Post Archean Average Australian Shale (PAAS)-normalized (Taylor and McLennan ,1985) multi-element spider diagram of phyllites of DVSB. **(d)** Geochemical classification of low-grade metasedimentary rocks from Dalma volcano-sedimentary basin using the diagram log ($SiO_2/Al_2O_3$) vs log ($Fe_2O_3/K_2O$) (after Herron 1988).

($Al_2O_3$+CaO*+$Na_2O$) ratio, while the CIA index results from $Al_2O_3$/($Al_2O_3$+CaO*+$Na_2O$+$K_2O$) ratio, with CaO* including only Ca associated with silicate minerals. Most of the analyzed samples show consistent loss-on-ignition (LOI) and low CaO values; hence the presence of significant amounts of carbonates is ruled out. Thus, the variable CIA and CIW values indicate that these rocks were exposed to moderate to high degree of chemical weathering. The triangular diagram $Al_2O_3$-Cao*+$Na_2O$-$K_2O$ (A-CN-K) diagram shows the weathering trend of the sediments (Fedo et al.1995). The samples exhibit a linear pattern towards the $Al_2O_3$ axis, which implies an advanced paleoweathering trend (Fig.4a). The extent of paleoweathering has also been assessed using the $K_2O$-$Fe_2O_3$-$Al_2O_3$ ternary diagram (Fig. 4b) (Wronkiewicz and Condie 1987). In this diagram, most samples cluster near the residual clay field and indicate high degrees of paleoweathering. Significantly one sample with high CIA value, exhibits lesser degree of source area weathering on this ternary diagram. This phenomenon is attributed to the in-situ chemical weathering of sediments (post-depositional alteration) within these samples.

The weathering index of Parker (WIP) was calculated after Parker 1970. The WIP values ranges between 13 to 49, which is considerably lower than the CIA values. However, these low WIP reflect moderate to high degree of weathering for the carbonaceous host rocks (Gonzalez et al. 2017). In the CIA vs. WIP diagram, the sample values lie within the moderate to intense weathering fields (Fig. 4c); which is in agreement to the A-CN-K diagram (Fig. 4a).

## Trace Elements

Trace element concentrations are listed in Table 2. The trace element distribution indicates the enrichment of incompatible elements over compatible elements. A predominant enrichment of the incompatible elements suggests a felsic provenance for these meta-sedimentary units. The Th/Sc and Zr/Sc ratios show a strong positive correlation in sedimentary rocks (Fig.5a). However, physical weathering of clastic rocks during multiple recycling events, results in a marked increase in the Zr/Sc ratios. The Zr/Sc values support sediment sorting and recycling, as higher Zr content indicates higher Zr input within the sedimentary succession which is a consequence of increased sedimentary sorting and recycling. The Th/Sc ratio however, is not significantly affected by such processes. Thus, the Th/Sc vs Zr/Sc ratio can be used as a proxy to determine the effect of diverse sedimentation cycles. Hence, the Th/Sc vs Zr/Sc diagram has been used to evaluate the effect of sediment recycling. The high Zr content within these phyllites has been assessed from the PAAS normalized

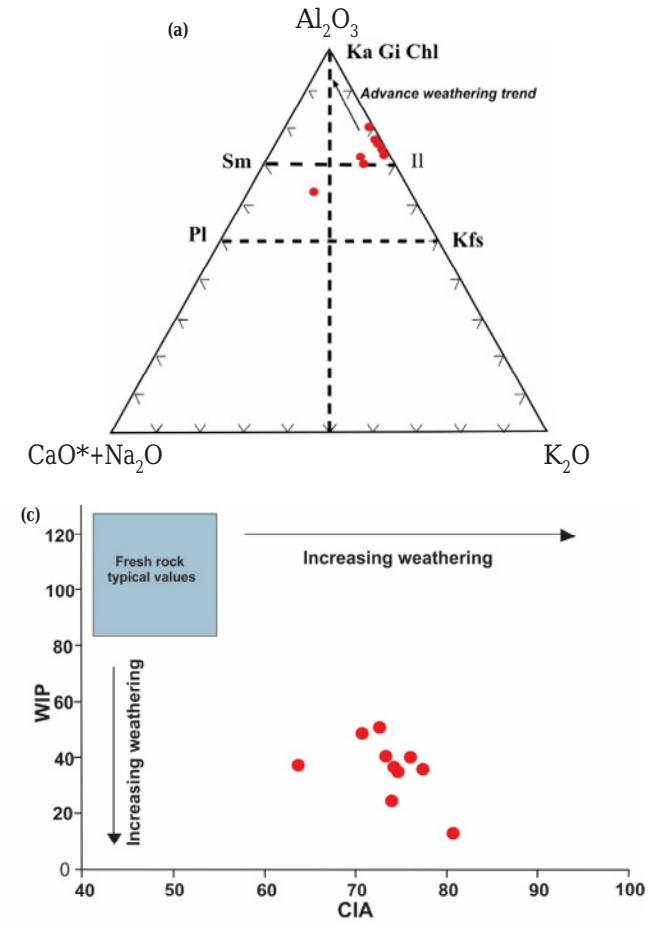


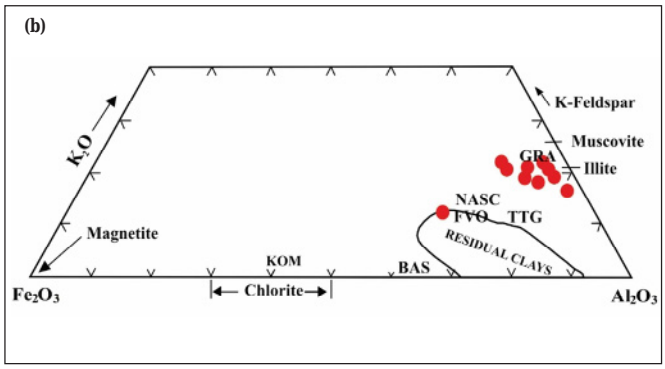


**Fig.4. (a)** Chemical Index of alteration (CIA) diagram (after Nesbitt and Young, 1982, 1984) showing the weathering trend for the studied samples. Mineral abbreviations: Kaol: kaolinite, Il: Ilite, Kfsp: potash feldspar, Pl:plagioclase, Sm:Smectite, Gi:Gibsite. **(b)** $K_2O$-$Fe_2O_3$-$Al_2O_3$ ternary plot adapted from Wronkiewicz and Condie (1987). Field of residual clays is from Reimer (1985). Abbreviations stand for the KOM=Komatiite; BAS=Basalt; NASC=North American Shale Composite; TTG = Tonalite/Trondhjemite/granodiorite; GRA=Granite; FVO=Felsic volcanic. **(c)** Relationship between two weathering proxies, CIA (Nesbitt and Young, 1984) and WIP (Parker, 1970) for metasedimentary rocks of Dalma volcano-sedimentary rocks.

trace element distribution diagram (Fig.5b). In this figure, a predominant increase in Zr content is observed with respect to other elements (Fig.5b). The carbonaceous rocks of the DVSB exhibit Th/Sc ratios between 0.62 to 6.9 whereas Zr/Sc values range from 8.65 to 14.55 which suggests that these rocks underwent moderate degree of mechanical weathering.

## PROVENANCE CHARACTERIZATION

### Evidence from Major Oxides

The discrimination binary diagram of DF1 vs DF2 functions by Roser and Korsch 1988, shows that most of the analyzed samples fall within the quartzose sedimentary provenance, except one sample (CP- 9) which indicates a felsic igneous provenance (Fig.6a).

### Evidence from Trace Elements

The analyzed metasedimentary units reveal Th/Co values >0.5 and La/Sc ratios >1.2, which reflects a felsic source component for these rocks (Fig.6b) (Cullers, 2002). The ocassional enrichement of Co might be a consequence of replacement of $Fe^{2+}$ by Co in detrtial pyrite (Ghosh et al. 2016). The REE pattern (Fig.6c) of the analyzed samples show enriched LREE and a flat HREE pattern along with negative Eu anomaly (normalized to C1 chondrite, after McDonough and Sun, 1995) (C1 chondrite normalized Eu/Eu* <1). The metasedimentary rocks also reveal fractionated REE pattern ($La_N/Yb_N$=3.8-8). Europium anomaly generally exhibits the tendency

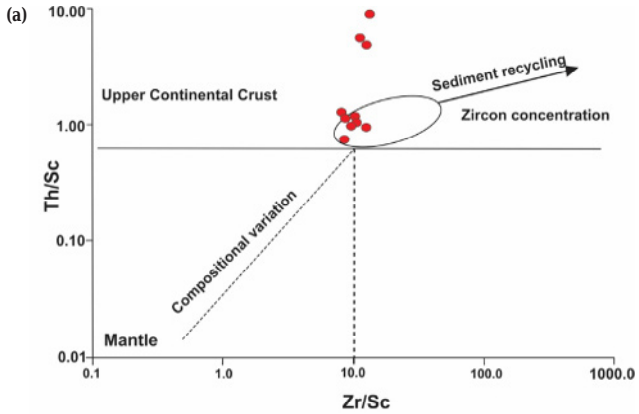


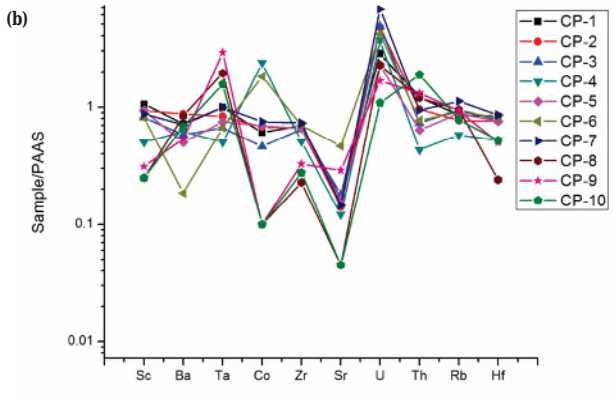


**Fig.5. (a)** Th/Sc vs Zr/Sc diagram after McLennan et al. (1993) indicating recycling, sedimentary sorting and upper crustal input. High Zr/Sc ratios imply higher degree of reworking. **(b)** PAAS-normalised spider diagram for trace elements of metasedimentary rocks of Dalma volcano-sedimentary basin.

**Table 2.** Trace elements concentration and critical elemental ratios of the metasedimentary units, analyzed by ICPMS (Analysis carried out at Bureau Veritas Commodities Ltd. Vancouver, Canada laboraties) and SAIF, IIT-Bombay

| Elements | CP-1 | CP-2 | CP-3 | CP-4 | CP-5 | CP-6 | CP-7 | CP-8 | CP-9 | CP-10 |
|---|---|---|---|---|---|---|---|---|---|---|
| Sc (ppm) | 17 | 15 | 13 | 8 | 15 | 13 | 14 | 4 | 5 | 4 |
| V (ppm) | 479 | 371 | 840 | 1179 | 473 | 225 | 721 | 144 | 129 | 54 |
| Ba (ppm) | 470 | 570 | 379 | 402 | 325 | 120 | 462 | 548 | 347 | 445 |
| Sn (ppm) | 3 | 3 | 2 | 1 | 3 | 0 | 3 | 1 | 2 | 2 |
| Y (ppm) | 39 | 31 | 44 | 33 | 17 | 24 | 44 | 10 | 12 | 11 |
| Zr (ppm) | 147 | 139 | 136 | 107 | 138 | 147 | 154 | 48 | 69 | 58 |
| Sr (ppm) | 33.2 | 28.2 | 35.9 | 24.3 | 32.6 | 93.1 | 29.2 | 9.02 | 57.62 | 9.02 |
| Cr (ppm) | 0.082 | 0.0088 | 0.0171 | 0.0136 | 0.0082 | 0.006 | 0.015 | 0 | 0 | 0 |
| Co (ppm) | 13.9 | 15.6 | 10.6 | 54.9 | 16 | 42 | 17.3 | 0 | 0 | 0 |
| Ni (ppm) | <20 | <20 | <20 | <20 | <20 | <20 | <20 | <20 | <20 | <20 |
| Cu (ppm) | 86.6 | 44.5 | 38.4 | 67.4 | 12.1 | 13.5 | 13.3 | 10.25 | 42.6 | 28.7 |
| Zn (ppm) | 8 | 44 | 4 | 5 | 22 | 127 | 15 | 6 | 4 | 14 |
| Ga (ppm) | 17.7 | 17.6 | 14.3 | 10.3 | 15 | 12.1 | 14.9 | 13.5 | 16.4 | 9.7 |
| Rb (ppm) | 136.3 | 122.8 | 151.9 | 92.9 | 141.3 | 146 | 179.4 | 152.4 | 148.6 | 125.8 |
| Nb (ppm) | 14 | 11.4 | 9.7 | 8.7 | 11 | 10.4 | 12 | 9.22 | 9.23 | 2.84 |
| Cs (ppm) | 13.9 | 15.6 | 10.6 | 54.9 | 16 | 42 | 17.3 | 14.5 | 39.8 | 15.2 |
| Pr (ppm) | 5.12 | 9.44 | 3.62 | 3.88 | 3.14 | 6.78 | 5.01 | 5.58 | 6.64 | 6.54 |
| Nd (ppm) | 17.1 | 33.5 | 12.9 | 16.3 | 10.2 | 25.4 | 19.4 | 22.17 | 23.76 | 22.4 |
| Sm(ppm) | 3.2 | 6.29 | 2.87 | 3.25 | 1.74 | 4.62 | 3.93 | 3.34 | 4.28 | 4.06 |
| Eu(ppm) | 0.68 | 1.29 | 0.72 | 0.88 | 0.44 | 1.04 | 0.94 | 1.07 | 0.97 | 1.03 |
| Gd(ppm) | 3.15 | 5.41 | 3.99 | 4.04 | 2.04 | 4.45 | 4.96 | 4.84 | 4.53 | 4.57 |
| Tb(ppm) | 0.63 | 0.85 | 0.79 | 0.64 | 0.4 | 0.69 | 0.9 | 0.66 | 0.71 | 0.73 |
| Dy(ppm) | 4.55 | 5.18 | 5.41 | 4.25 | 2.63 | 4.27 | 6 | 5.13 | 4.53 | 6.05 |
| Ho(ppm) | 1.15 | 1.1 | 1.32 | 1.04 | 0.66 | 0.91 | 1.43 | 0.96 | 0.97 | 1.35 |
| Er(ppm) | 3.88 | 3.22 | 4.09 | 3.13 | 1.92 | 2.65 | 4.33 | 4.32 | 2.94 | 2.68 |
| Tm(ppm) | 0.57 | 0.5 | 0.56 | 0.44 | 0.32 | 0.38 | 0.65 | 0.54 | 0.49 | 0.65 |
| Yb(ppm) | 3.63 | 3.26 | 3.49 | 2.76 | 1.98 | 2.57 | 4.06 | 4.02 | 3.36 | 3.29 |
| Lu(ppm) | 0.55 | 0.52 | 0.53 | 0.43 | 0.32 | 0.38 | 0.6 | 0.66 | 0.53 | 0.41 |
| Hf(ppm) | 4.2 | 3.8 | 3.9 | 2.6 | 3.8 | 4.1 | 4.3 | 1.2 | 2.5 | 2.6 |
| Ta(ppm) | 1.2 | 1 | 0.8 | 0.6 | 0.9 | 0.8 | 1.2 | 2.34 | 3.49 | 1.88 |
| Pb(ppm) | 96 | 77.3 | 35.7 | 8.2 | 9.6 | 19.1 | 20.1 | 15.4 | 36.2 | 11.4 |
| Th(ppm) | 17.8 | 14.1 | 10.7 | 6.3 | 9.3 | 11.3 | 13.8 | 17.5 | 19.2 | 27.6 |
| U(ppm) | 6 | 9.9 | 10.1 | 7.7 | 4.8 | 8.7 | 14.1 | 4.8 | 3.5 | 2.29 |
| U/Th | 0.33 | 0.70 | 0.94 | 1.22 | 0.51 | 0.76 | 1.02 | 0.27 | 0.18 | 0.08 |
| Th/Sc | 1.04 | 0.94 | 0.82 | 0.78 | 0.62 | 0.86 | 0.98 | 4.37 | 3.84 | 6.9 |
| Zr/Sc | 8.65 | 9.29 | 10.46 | 13.48 | 9.24 | 11.32 | 11.05 | 12.2 | 13.84 | 14.55 |
| La/Th | 1.80 | 3.36 | 2 | 2.80 | 2.07 | 2.69 | 1.68 | 1.39 | 1.23 | 0.88 |
| Cr/Th | 0.000985 | 0.001348 | 0.003415 | 0.00464 | 0.001886 | 0.001293 | 0.002463 | 0 | 0 | 0 |
| La/Sc | 1.88 | 3.16 | 1.64 | 2.21 | 1.28 | 2.34 | 1.66 | 6.08 | 4.76 | 6.11 |
| Eu/Eu* | 0.023 | 0.013 | 0.021 | 0.023 | 0.042 | 0.017 | 0.016 | 0.04 | 0.017 | 0.016 |

of Eu to be incorporated into plagioclase over other minerals. Due to plagioclase fractionation during the early phase of magma crystallization, most of the Eu is incorporated into plagioclase, which causes a positive Eu anomaly, whereas rest of the magma remains relatively depleted in Eu and hence exhibits a negative Eu anomaly. A negative Eu anomaly also suggests derivation of sediments from felsic sources (Cullers 1995). The negative Ce anomaly in the REE pattern, may be attributed to the prolonged sub-aquatic weathering (Kuster and Liegeois 2001) or by post depositional alteration such as progressive circulation of hydrothermal fluids (Abouchami et al. 1990). It may also be inherited from the source rocks (Shimizu et al. 1992). Cerium oxidizes in seawater from the $3^+$ to the more insoluble $4^+$ oxidation state, resulting in an overall enrichment of Ce relative to other REE's (Cullers 2002). Hence, a negative Ce anomaly may be indicative of reducing ocean water conditions. In the Eu/Eu* vs Th/Sc (Fig.6d) disciminantion diagram, our studied samples show a cluster in the field, which corresponds to a source of evolved felsic composition (Jorge et al., 2013).

## TECTONIC SETTING

### Evidences from Major Elements

Major element discriminant plots such as $\log(K_2O/Na_2O)$ versus $SiO_2$ and $SiO_2/Al_2O_3$ versus $\log(K_2O/Na_2O)$ were used to discriminate between different tectonic regimes (Fig.7a, b). In both the plots, majority of the samples fall within the passive margin setting whereas few samples lie along the boundary between active continental margin and passive margin. In the $TiO_2$ vs. $(Fe_2O_3+MgO)$ plot (Fig.7c), the samples occupy the passive margin field (Bhatia 1983). In the DF1 vs DF2 diagrams well (Bhatia 1983) (Fig.7d),all the samples fall within the passive margin field(Roser and Korsch, 1988).

### Evidences from Trace Elements

Trace elements like Th, Sc, La and Zr are useful for the discrimination of provenance and tectonic setting because of their short residence time in sea water and lower mobility during sedimentary processes (Holland 1978; McLennan et al. 1983; Bhatia and Crook

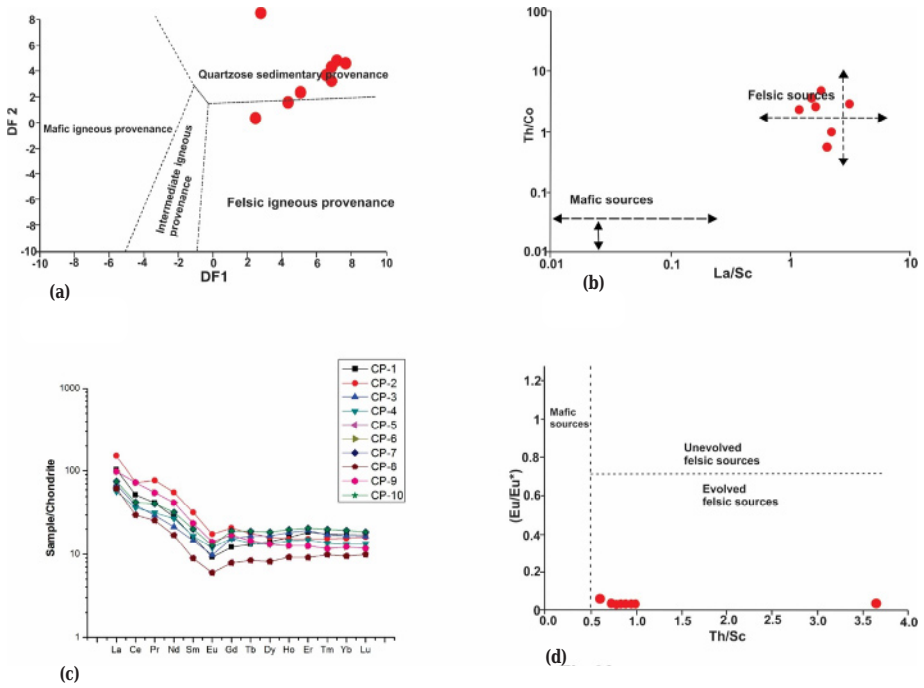


**Fig.6. (a)** Discrimination diagram for sedimentary provenance (after Roser and Korsch 1988), DF1= 30.638 $TiO_2/Al_2O_3$ - 12.541 $Fe_2O_3/Al_2O_3$+ 7.329 $MgO/Al_2O_3$+ 12.031 $Na_2O/Al_2O_3$ + 35.402 $K_2O/Al_2O_3$ - 6.382. DF2 =-56.5 $TiO_2/Al_2O_3$-10.879 $Fe_2O_3/Al_2O_3$+ 30.875 $MgO/Al_2O_3$-5.404$Na_2O/Al_2O_3$+11.112 $K_2O/Al_2O_3$-3.89. **(b)** Th/Co vs La/Sc diagram for provenance discrimination (after Cullers 2002). **(c)** Chondrite-normalized REE patterns for metasedimentary rocks of Dalma volcano-sedimentary formation. **(d)** Eu/Eu* (chondrite-normalized) vs Th/Sc plot showing the distribution of studied samples derived from mafic and felsic igneous sources (after McLennan et al. 1990; Cullers, 2002).

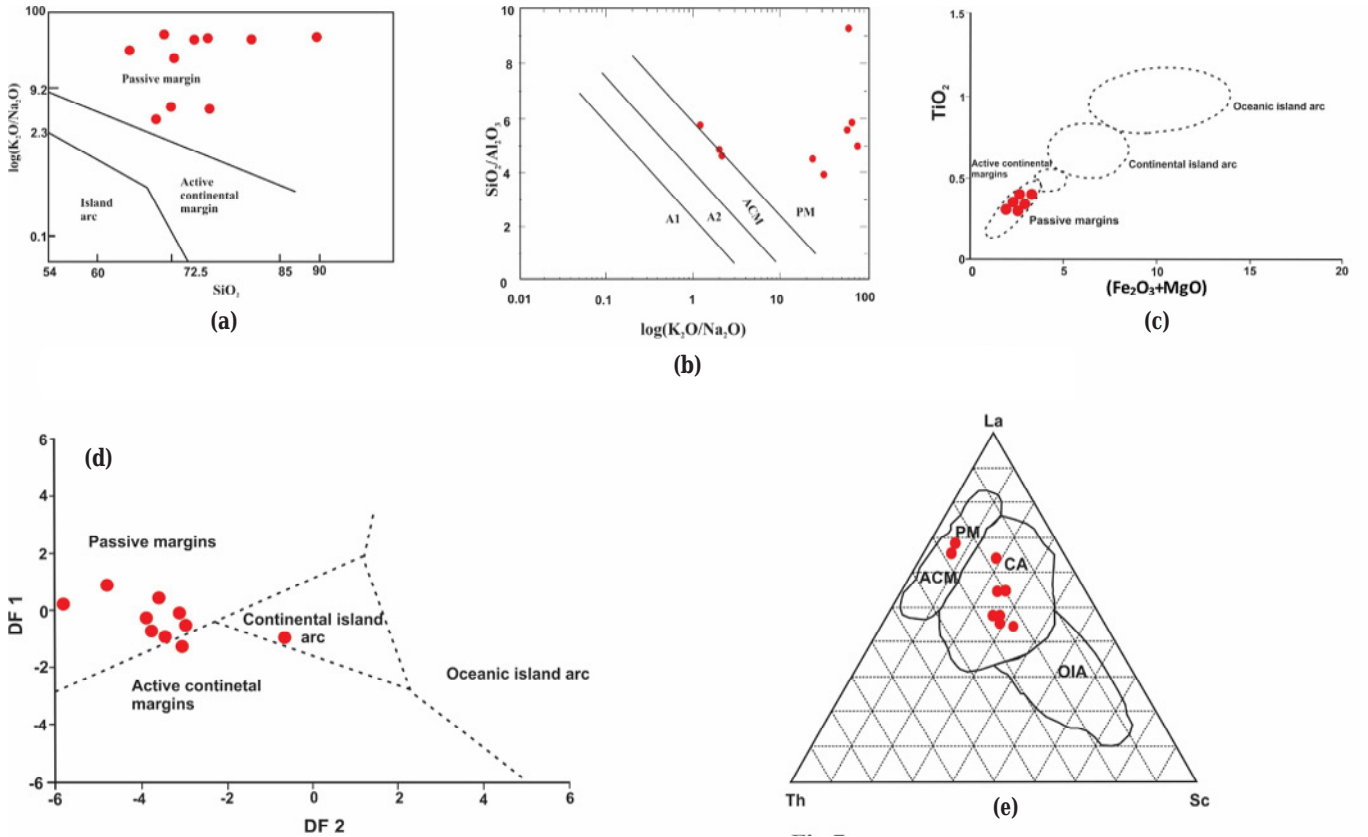


**Fig.7. (a)** Tectonic discrimination diagram $SiO_2$ vs $\log(K_2O/Na_2O)$ (after Roser and Korsch 1986) showing deposition of studied metasedimentary rocks in a passive margin setting. **(b)** Tectonic discrimination diagram $SiO_2/Al_2O_3$ vs log ($K_2O/Na_2O$) (after Maynard et al.1982) PM=Passive margin, ACM=Active continental margin , A1=Arc setting, basaltic and andesitic detritus, A2=evolved arc setting, felsic plutonic detritus. Studied metasedimentary rocks fall within the passive margin setting. **(c)** Plot of $Fe_2O_3$+MgO vs $TiO_2$ to discriminate tectonic setting (after Bhatia 1983). **(d)** Major elements composition of metasedimentary rocks of studied area used for discriminate tectonic setting (after Bhatia 1983). DF1=-0.421 $SiO_2$+1.988 $TiO_2$- 0.526 $Al_2O_3$ -0.551 $Fe_2O_3$- 1.610 FeO + 2.720 MnO + 0.881 MgO - 0.907 CaO - 0.177 $Na_2O$ - 1.840 $K_2O$ +7.244 $P_2O_5$ +43.57. DF2=-0.0447 $SiO_2$- 0.972 $TiO_2$+ 0.008 $Al_2O_3$-0.267 $Fe_2O_3$+ 0.208 FeO -3.082 MnO + 0.140 MgO + 0.195 CaO + 0.719 $Na_2O$ - 0.032 $K_2O$ + 7.510 $P_2O_5$+ 0.303. **(e)** La-Th-Sc plot for the metasedimenatry rocks from Dalma volcano-sedimentary rocks for tectonic setting (after Bhatia and Crook 1986) PM-Passive margin, ACM-Active continental margin, CA-Continental island arc, OIA-Oceanic island arc.

1986). In the La-Th-Sc triangular diagram (Fig.7e) the analyzed samples plot within the passive margin setting, in agreement to the major element tectonic decimation diagrams. Majority of the tectonic setting diagrams, using geochemical data of clastic rocks are based on data collected from Phanerozoic rock suites. Based on paleomagnetic, geochemical, and tectonostratigraphic data, Cawood et al. (2006) established the presence of plate tectonics since at least 3.1 Ga, and also that the Precambrian lithospheric plates were similar to the Phanerozoic in terms of their tectonic setup. However, application of these methods to Precambrian rocks are still a matter of debate, and does have its limitations; as the evolution of the Archean continental crust took place in different magmatic conditions and tectonic regimes compared to the Proterozoic and Phanerozoic crust. Nevertheless, apart from the tectonic discrimination diagrams used in this study, several trace elements and selected major element data from these metasedimentary sequences exhibit similarity with modern-day passive continental margin, with characteristic signatures of sedimentary recycling. Trace element ratios such as Th/Sc, La/Sc and Cr/Th indicate sediment derivation from passive margins i.e., from intracratonic felsic sources (McLennan and Taylor 1991; Ghosh et al. 2016). Also, the variable Zr/Sc ratios in these rocks indicate sediment recycling; a common phenomenon associated with intracratonic settings.

## CONCLUSIONS

In this work, various geochemical proxies such as major element data, trace element ratios, and REE concentrations were used to deduce the geochemical characteristics of the metasedimentary units of the DVSB. The study also provides a comprehensive report on the paleo-weathering characteristics, nature of source region and the tectonic set up of these Au-bearing metasedimentary rocks. Field and petrographic studies reveal that post-depositional alteration within these phyllites is prevalent only near the major faults. Such areas are manifested by widespread silicification and were avoided while collecting samples. A post-depositional alteration event, induced by late stage fluids follow certain fluid pathways and exhibit zonation patterns that mark dispersion of the fluid pathway (Nwaila et al., 2017). Such dispersion/alteration haloes are neither observed in the field, nor reported previously by any worker. Although sericite is observed in a few samples, its occurrence is rare and is not widespread. We speculate small-scale alterations as a consequence of local fluid migration related to the low-grade metamorphism in these rocks. The major oxide data reveals a clear predominance of $SiO_2$; and the CIA and WIP suggest intense chemical weathering in the source region, coupled with moderate to high degree of mechanical weathering. The idea of mechanical weathering is further supplemented by petrographic observations and moderate Zr/Sc ratios, which suggest sediment sorting and recycling. A high degree of chemical weathering of the protolith is suggested by the A-CN-K diagram, where majority of the samples plot along the A-K line of the diagram. The uniform U/Th ratios (Table 2) are indicative of limited post-depositional alteration within these samples. Uranium, although much more mobile than Th, shows a fairly uniform ratio with Th in all the samples. This phenomenon can be ascribed to limited post depositional alteration, which otherwise would have resulted in widespread removal of U from the samples. Hence, we infer that post-depositional alterations in these samples are volumetrically far less significant as compared to alterations related to paleoweathering. Given the evidences against significant post-depositional alteration, we conclude that the variable CIA and CIW values are an artifact of differential chemical weathering in the source area.

Considering the fact that these metasedimentary units suffered limited post-depositional alteration, we have utilized selected trace elements (including REE) to decipher the provenance characteristics and tectonic affinity of these units. The REE data reveals enriched LREE and a flat HREE pattern with negative Eu anomaly. This implies that the protolith to these metasedimentary rocks were produced from intra crustal melting in which feldspar (mainly Ca-plagioclase) with abundant Eu is left over in the residue. This provides strong evidences in favor of a felsic source region. The felsic provenance is further supported by the moderate to high Th/Sc ratios and an overall enrichment in the incompatible elements. In the tectonic discrimination diagrams, majority of the samples occupy the passive margin field with some samples having a continental arc affinity. Field observations including lithology and structure, coupled with geochemical data from the the metasedimentary units of the DVSB indicates an evolutionary pattern close to a passive margin setting. Based on these observations, we propose that the Archean Singhbhum granite complex, lying to the south of the NSMB, was the dominant source for these studied metasediments. The moderate degree of mechanical weathering suggests a prolonged period of slow uplift and erosion of the Singhbhum granite.

*Acknowledgments:* Authors are thankful to the Director, Indian Institute of Technology (Indian School of Mines) Dhanbad for providing necessary permission to carry out the research work. MK greatly acknowledges the financial support received from IIT (ISM) Dhanbad in the form of research fellowship. Thanks are also due to the Department of Science and Technology, Ministry of Science and Technology, Govt. of India for some of the facilities availed vide project number NRDMS/01/07/014. Authors are also thankful to Bureau Veritas Commodities Ltd (Vancouver, Canada), and SAIF IIT, Bombay for carrying out whole rock geochemical analysis. Thanks are also due to the editor, Prof. B. Mahabaleswar for editorial guidance. Authors are also grateful to the two anonymous reviewers for providing valuable comments and suggestions that has immensely improved the manuscript.

**References**

Abouchami, W., Boher., M, Michard, A., and Albarede, F. (1990) A major 2.1 Ga old event of mafic magmatism in West Africa: An early stage of crustal accretion. Jour. Geophys. Res., v.95, pp.17605–17629.

Bhatia, M.R. (1983) Plate tectonics and geochemical composition of sandstones. Jour. Geol., v.91, no.6, pp.611-627.

Bhatia, M.R. and Crook, K.A.W. (1986) Trace element characteristics of greywackes and tectonic settling discriminations of sedimentary basins. Contrib. Mineral. Petrol., v.92, pp.181-193.

Cawood, P., Kroner, A. and Pisarevsky, S.A. (2006) Precambrian plate tectonics: Criteria and evidence. GSA Today, v.16(7), pp.4-10.

Chakravarti, R., Singh, S., Venkatesh, A.S., Patel, K. and Sahoo, P.R. (2018) A modified placer origin for refractory gold mineralization within the Archean radioactive quartz-pebble conglomerates from the eastern part of the Singhbhum Craton, India. Econ. Geol. v.113(2), pp.579-596.

Condie, K.C., Noll, P.D., and Conway, C.M. Jr. (1992) Geochemical and detrital mode evidence for two sources of early Proterozoic sedimentary rocks from the Tonto Basin Supergroup, central Arizona. Sediment. Geol., v.77, pp.51–76.

Cruz-Gamez,E.M., Velasco-Tapia,F., Ramirez-Fernandez, J.A., Jenchen, U., Rodriguez-Saavedra, P., Rodriguez-Diaz, A.A. and Iriondo.A. (2017) Volcanic sequence in Late Triassic-Jurassic siliciclastic and evaporitic rocks from Galeana, NE Mexico. Geologica Acta, v.15(2) pp.89-106.

Cullers, R. (1995) The controls on the major-and trace-element evolution of shales, siltstones, and sandstones of Ordovician to Tertiary age in the Wet Mountains 261 region, Colorado, USA. Chem. Geol., v.123, pp.107-131.

Cullers, R.L. (2000) The geochemistry of shales, siltstones and sandstones of Pennsylvanian Permian age, Colorado, USA: implications for provenance and metamorphic studies. Lithos 51, 181-203

Cullers, R. (2002) Implications of elemental concentrations for provenance, redox conditions, and metamorphic studies of shales and limestones near Pueblo, CO, USA. Chem. Geol., v.191, pp.305-327.

Cullers, R. L., and Podkovyrov, V. N. (2000) Geochemistry of the Mesoproterozoic Lakhanda shales in southeastern Yakutia, Russia:

implications for mineralogical and provenance control, and recycling. Precambrian Res., v.104(1), pp.77-93.

Das, B. K., Al-Mikhlafi, A. S., and Kaur, P. (2006) Geochemistry of Mansar Lake sediments, Jammu, India: Implication for source-area weathering, provenance, and tectonic setting. Jour. Asian Earth Sci., v.26, pp.649–668.

Dunn, J.A., and Dey, A.K. (1942) The geology and petrology of Eastern Singhbhum and surrounding areas. Mem Geol. Surv. India, v.69(2), pp.281-456.

Fedo, C.M., Nesbitt, H.W., and Young, G.M. (1995) Unraveling the effects of potassium metasomatism in the sedimentary rocks and paleosols with implications for paleoweathering conditions and provenance. Geol., v.23, pp.921-924.

Ghosh, S., De, S. and Mukhopadhyay, J. (2016) Provenance of >2.8 Ga Keonjhar quartzite, Singhbhum Craton, Eastern India: Implications for the Nature of Mesoarchean Upper Crust and Geodynamics. Jour. Geol., v.124 (3), pp.331–351.

Gonzalez, P.A.A., Garben, G., Hauser, N. and Gigena, L. (2017) Geochemistry of metasedimentary rocks from Puncoviscana complex in the Mojotoro Range, NW Argentina: Implication for provenance and tectonic setting. Jour. South Amer. Earth Sci., v.78 , pp.250-263.

Gupta, A., and Basu, A. (2000) North Singhbhum Proterozoic mobile belt, Eastern India-A Review. Geol. Surv. India, Spec. Pub., v.55 pp.195-226.

Gupta, A., Basu, A., and Ghosh, P, K. (1982) Ultramafic volcaniclastics of the Precambrian Dalma Volcanic Belt, Singhbhum, Eastern India. Geol. Mag., v.119, pp.505-510.

Herron, M.M. (1988) Geochemical classification of terrigenous sand and shales from core or log data. Jour. Sed. Res., v.58, pp.820-829.

Holland, H.D. (1978) The Chemistry of the Atmosphere and Oceans. Wiley, New York, 351p.

Jha, V., Singh, S. and Venkatesh, A.S. (2015) Invisible Gold Occurrence within the Quartz Reef Pyrite of Babaikundi Area, North Singhbhum Fold and Thrust Belt, Eastern Indian Shield: Evidences from Petrographic, SEM and EPMA Studies. Ore Geol. Rev., v.65, pp.426-432.

Jorge, R.C.G.S., Fernandes, P., Rodeigues, B., Pereira, Z. and Oliveira, J.T. (2013) Geochemistry and provenance of the carboniferous Baixo Alentejo Flysch Group, South Portuguese Zone. Sedimentary Geol., v.284-285, pp.133-148.

Khatun, M., and Singh, S. (2018) Genesis of the sulfide hosted refractory gold occurrences within the carbonaceous metasedimentary units of the Dalma volcano-sedimentary basin, North Singhbhum mobile belt, eastern India. Jour. Geol. Soc. India., v.92, pp.11-18.

Kûster, D. and Liëgeois, J.P. (2001) Sr, Nd isotope and geochemistry of the Bayuda Desert high grade metamorphic basement (Sudan): an early Pan-African oceanic convergent margin, not the edge of the East Sahara ghost craton? Precambrian Res., v.109, pp.1-23.

Lima, M.M.C., Silva, T.R., Ferreira, V.P., and Silva., J.M.R. (2014) Metasedimentary rocks of the northern portion of the Macurure domain, Sergipano belt,northern Brazil: Geochemical characterization of their protoloths and tectonic implications, Estudos Geologicos, v.24 no.2,pp.89-107.

Mahadevan, T.M. (2002) Geology of Bihar and Jharkhand. Geological Society of India, Bangalore, pp.169-230.

Maurya, V.P., Shalivahan, Bhattacharya, B.B., Adhikari, P.K., and Das, L.K. (2015) Preliminary Magnetotelluric Results across Dalma Volcanic, Eastern India: Inferences on Metallogeny. Jour. Appld. Geophys., v.115, pp.171-182.

Maynard, J.B., Valloni, R. and Yu, H.-S.(1982) Composition of modern deep sea sands from arc-related basins. *In:* J.K. Legget (Ed.), Trench-Forearc Geology. Geol. Soc. Spec. Publ., v.10 pp.551-561.

Mazumder, R. (2000) Turbulance-particle Interactions and their Implications for Sediment Transportand Bedform Mechanics under Unidirectional Current; Some Recent Developments. Earth Sci. Rev., v.50, pp.113-124.

Mazumder, R. (2003) Correlations between the Eastern Block of the North China Craton and the South Indian Block of the Indian Shield: an Archaean to Paleoproterozoic link-comment. Precambrian Res., v.127, pp.379-380.

Mcdonough, W.F., and Sun, S., (1995) Composition of the earth. Chem. Geol., v.120, pp.223-253.

Mclennan, S., Taylor, S., and Krõner, A. (1983) Geochemical evolution of Archean shales from South Africa I. The Swaziland and Pongola Supergroups. Precambrian Res., v.22 pp.93-124.

Mclennan, S.M. Taylor, S.R. Mcculloch, M.T. and Maynard, J.B. (1990) Geochemical and Nd-Sr isotopic composition of deep-sea turbidites: Crustal evolution and plate tectonic associations. Geochim. Cosmochim. Acta, v.54(7), pp.2015-2050.

Mclennan, S.M. and Taylor, S.R. (1991) Sedimentary rocks and crustal evolution: tectonic setting and secular trends. Jour. Geol., v.99,(1), pp.1-21.

Mclennan, S., Hemming, S., Mcdaniel, D., and Hanson, G. (1993) Geochemical approaches to sedimentation, provenance, and tectonics. *In:* Johnson, M., Basu, A. (Eds.), Processes Controlling the Composition of Clastic Sediments. Geol. Soc. Amer. Spec. Paper, v.284, pp.21-40.

Mukhopadhaya, D. (1990) Precambrian Plate Tectonics in the Eastern Indian Shield. *In:* Synchanthavog S.P.H. (Ed.) Crustal evolution and orogeny. Oxford: IHB Publ. Co., pp.75-100.

Mukhopadhaya, D. (1994) Evolution of the Precambrian Terrane of Singhbhum. Extended abstract, Symp on mantle dynamics and its relation to earthquakes and volcanism, Calcutta, pp.45-48.

Nelson, D.R., Bhattacharya, H.N., Misra, S., Dasgupta, N., and Altermann, W. (2007) New Shrimp U-Pb dates from the Singhbhum Craton, Jharkhand-Orissa region, India. (Abst.) Int.Conf. on Precambrian Sediments and Tectonics. 2nd GPSS meeting, IIT Bombay, pp.47.

Nesbitt, H.W., and Young, G.M. (1984) Early Proterozoic climates and plate motion inferred from major element chemistry of lutites. Nature, v.209, pp.715-717.

Nesbitt, H.W., and Young, G.M. (1984) Prediction of some weathering trends of plutonic and volcanic rocks based on thermodynamic and kinetic consideration. Geochim. Cosmochim. Acta, v.48, pp.1523-1534.

Nwaila, G., Frimmel, H.E. and Minter, W.E.L. (2017) Provenance and Geochemical variations in shales of the Mesoarchean Witwatersrand Supergroup. Jour. Geol., v.124(4), pp.399-422.

Parker, A. (1970) An index of weathering for silicate rocks. Geol. Mag., v.107, pp.501-504.

Reimer, T.O., (1985). Rare earth elements and the suitability of shales as indicators for the composition of the Archaean continental crust. Neues Jahrbuch fur Mineralogie-Abhandlungen, v.152, pp.211-223.

Roser, B.P. and Korsch, R.J. (1986) Determination of tectonic setting of sandstone693 mudstone suites using content and ratio. Jour. Geol., v.94(5), pp.635-650.

Roser, B.P. and Korsch, R.J. (1988) Provenance signatures of sandstone-mudstone suites determined using discriminant function analysis of major-element data. Chem. Geol., v.67(1-2), pp.119-139.

Roy, A., Sarkar, A., Jeyakumar, S., Aggarwal, S.K. and Ebihara, M. (2002b) Mid-Proterozoic Plume Related Thermal Event in Eastern Indian Craton: Evidence from Trace Elements, REE Geochemistry and Sr-Nd Isotope Systematic of Basic-Ultrabasic intrusive from Dalma Volcanic belt. Gondwana Res., v.5, pp.133-146.

Shimizu, H., Sawatari, H., Kawata, Y., Dunkley, P. N. and Masuda, A. (1992) Ce and Nd isotope geochemistry on arc volcanic rocks with negative Ce anomaly: existence of sources with on cave REE patterns in the mantle beneath the Solomon and Bonin island arcs. Contrib. Mineral. Petrol., v.110, pp.242–252.

Singh, S., Chandan, K.K. and Jha, V. (2018) Geochemistry of Paleo to Mesoproterozoic Metasedimentary Units of Chandil Formation, North Singhbhum Crustal Province: Implications for Provenance and Source Area Weathering. Jour. Geol. Soc. India., v.92, pp.166-172.

Taylor, S. R., And Mclennan, S. M. (1985) The continental crust: its composition and evolution. Oxford; Melbourne: Blackwell Scientific Publications.

Wan, B., Zhang, L., and Xiao, W. (2010) Geological and Geochemical Characteristics and Ore Genesis of Keketale VMS Pb-Zn Deposits, Southern Altai Metallogenic Belt, NW China. Ore Geol. Rev., v.37, pp.114-126.

Wronkiewicz.,D.J, and Condie,K.C.(1987) Geochemistry of Archean Shales from the Witwatersrand Supergroup, South Africa: Source-Area Weathering and Provenance. Geochim. Cosmochim. Acta, v.51, pp.2401-2416.

Zhang, M., Reilly, S.Y.O., Wang, K.I., Honsky, J., and Griffin, W.L. (2008) Flood Basalts and Metallogeny: the Lithospheric Mantle Connection. Earth Sci. Rev., v.86, pp.145-174.

*(Received: 17 May 2018; Revised form accepted: 7 February 2019)*